Inorganic Chemistry

Article

pubs.acs.org/IC

A Vacancy-Disordered, Oxygen-Deficient Perovskite with Long-Range Magnetic Ordering: Local and Average Structures and Magnetic Properties of $Sr_2Fe_{1.5}Cr_{0.5}O_5$

Farshid Ramezanipour,[†,‡] John E. Greedan,*[,†,‡] Joan Siewenie,[§] Ronald L. Donaberger,[⊥] Stuart Turner,[¶,∥] and Gianluigi A. Botton[‡,¶,▽]

[†]Department of Chemistry, and [‡]Brockhouse Institute for Materials Research, McMaster University, Hamilton, Canada L8S 4M

[§]Lujan Neutron Scattering Center, Los Alamos National Laboratory, Los Alamos, New Mexico 87545, United States

[⊥]Chalk River Laboratories, Canadian Neutron Beam Centre, National Research Council, Chalk River, Ontario, Canada K0J 1J0

[¶]Canadian Centre for Electron Microscopy, McMaster University, Hamilton, Canada L8S 4M1

[∥]EMAT, University of Antwerp, B- 2020 Antwerp, Belgium

[▽]Department of Materials Science and Engineering, McMaster University, Hamilton, Canada L8S 4M1

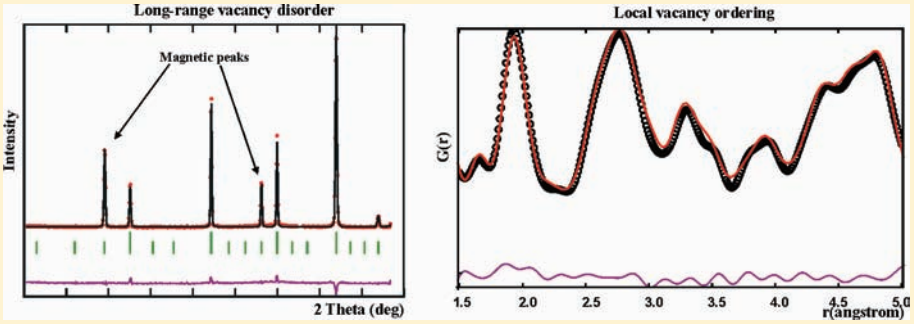

ABSTRACT: The local and average crystal structures and magnetic properties of the oxygen-deficient perovskite $Sr_2Fe_{1.5}Cr_{0.5}O_{5+y}$ were studied using powder X-ray and neutron diffraction, neutron-pair distribution function analysis, and electron energy-loss spectroscopy. This material crystallizes in the cubic $Pm\bar{3}m$ space group, with $a = 3.94491(14)$ Å. The oxygen vacancies are distributed randomly throughout the perovskite-type structure, and the average coordination number of the Fe(Cr) sites is 5. Refinement of the neutron diffraction data indicates $y \sim 0.05$. This is in discordance with an earlier report on a material with the same nominal composition and cell constant. Electron energy-loss Cr $L_{2,3}$-edge spectroscopy shows that Cr^{3+} is present, which is also contrary to previous speculation. Neutron-pair distribution function studies show that a brownmillerite-like model involving ordered vacancies and alternating octahedral and tetrahedral coordination at the metal sites, gives a better description of the local structure out to ~5 Å. A remarkable phenomenon determined by neutron diffraction in $Sr_2Fe_{1.5}Cr_{0.5}O_5$ is the occurrence of a long-range G-type antiferromagnetic ordering with $T_c \approx 565$ K because cubic oxygen-deficient perovskites with B-site disorder usually do not undergo transitions to magnetically ordered states. The observation of long-range antiferromagnetic order and the T_c value are in accordance with previous Mössbauer spectroscopic studies.

INTRODUCTION

In oxygen-deficient perovskites with formula $A_2BB'O_{6-y}$, $y \sim 1$, long-range ordering of oxygen vacancies may occur, resulting in a number of different structure types. The most common structure is brownmillerite, where the ordering of oxygen vacancies results in the formation of tetrahedral $B'O_4$ chains sandwiched between layers of apex-linked BO_6 octahedra. When magnetic ions are present on the B/B′ sites at concentrations above the percolation threshold, long-range magnetic ordering always accompanies the long-range vacancy ordering. On the contrary, the absence of vacancy ordering usually results in the destruction of the long-range magnetic ordering. For example, the ordered brownmillerite, Ca_2FeMnO_5, is antiferromagnetic with a G-type structure below $T_c = 407(2)$ K, while cubic Sr_2FeMnO_5 appears to be superparamagnetic at low temperatures.[1,2] In the oxygen-deficient cubic phases, long-range atomic disorder occurs on both the oxygen site and the small cation site, both of which presumably contribute to the quenching of long-range magnetic order. A recently reported example is cubic Sr_2FeScO_5, which exhibits a cluster glass ground state.[3] Interestingly, in many stoichiometric perovskites, $A_2B_{2-x}B_x'O_6$, disorder on the B sites alone also usually results in suppression of long-range magnetic order. An example is afforded by the materials Sr_2FeMO_6, where M = Nb and Sb. The M = Nb phase shows disorder on

Received: December 1, 2011
Published: January 30, 2012

   dx.doi.org/10.1021/ic202590r | *Inorg. Chem.* 2012, 51, 2638–2644

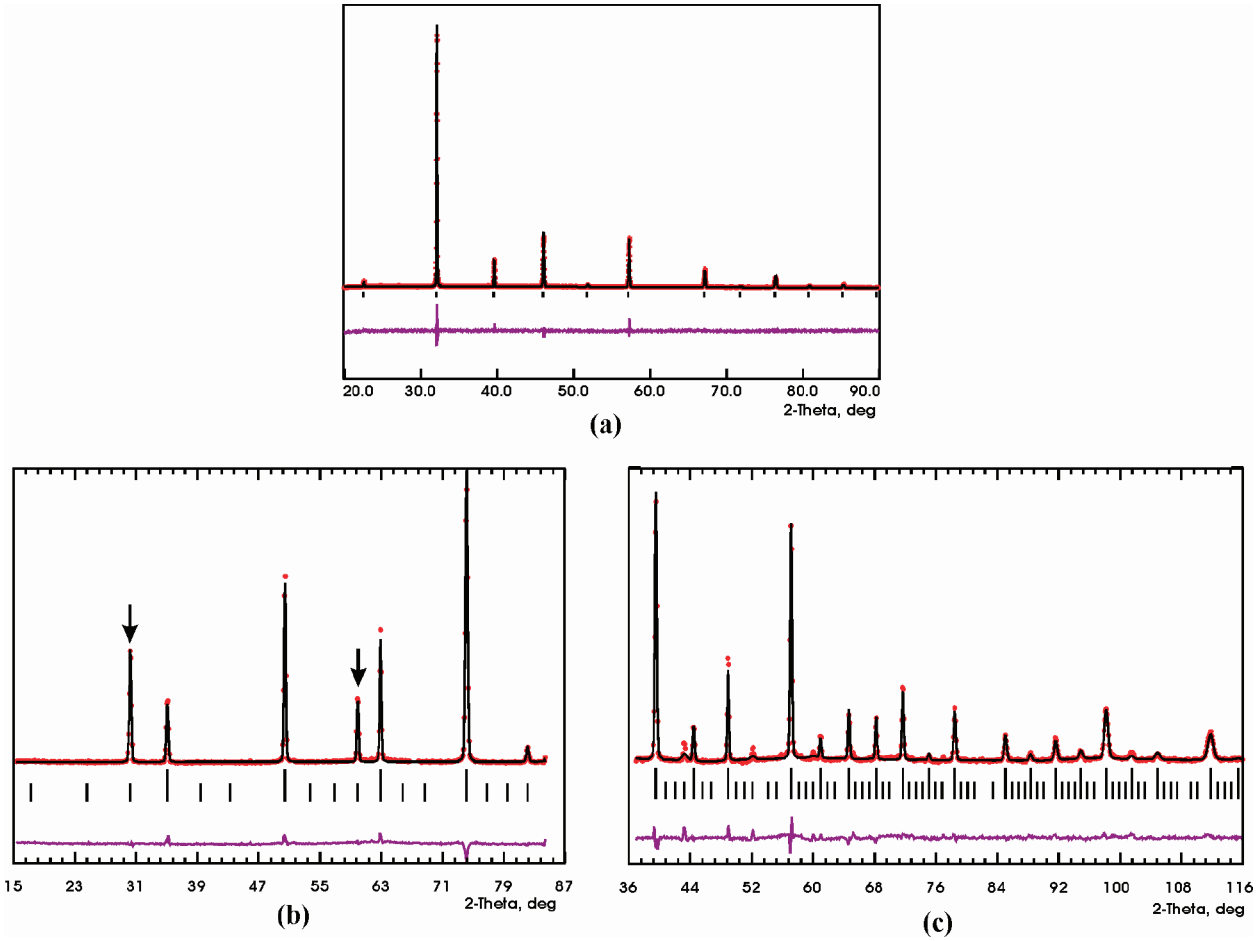

Figure 1. Rietveld refinement profiles for $Sr_2Fe_{1.5}Cr_{0.5}O_5$. The red circles are the experimental data, the solid line represents the model, the vertical tic marks locate the peak positions, and the lower solid line is the difference plot. (a) Powder X-ray diffraction (λ = 1.54056 Å) at 300 K. (b and c) Neutron diffraction, with λ = 2.3704 and 1.32829 Å, respectively, at 4 K. The neutron diffraction data show the presence of magnetic reflections. The main magnetic peaks are shown by arrows in part b. The neutron refinements involve both the crystal (upper tic marks) and magnetic structures (lower tic marks).

the B site (*Pbnm*) and is a spin glass, while the M = Sb phase shows at least partial B-site order ($P2_1/n$) and has an antiferromagnetic long-range-ordered ground state.[4,5] There are some exceptions; for example, A_2MnRuO_6, A = Ca and Sr, phases show no sign of B-site order yet exhibit various forms of long-range magnetic order.[6] Thus, reports of long-range magnetic order in perovskites with atomic disorder on both the oxygen and B-cation sites are extremely rare.

A number of studies have been reported for iron-based brownmillerites in which iron is partially substituted by another transition-metal element. The parent phases $Ca_2Fe_2O_5$ (*Pnma*) and $Sr_2Fe_2O_5$ (*Icmm*)[7−9] are both brownmillerites with long-range antiferromagnetic ordering. The brownmillerite structure is preserved upon substitution by cobalt to form Ca_2FeCoO_5[10] and Sr_2FeCoO_5.[11] Sr_2FeCoO_5 crystallizes in the *Imma* (*Icmm*) space group, similar to the parent compound $Sr_2Fe_2O_5$, because of the disorder of tetrahedral chain orientations. Concerning the calcium compounds, ordering of tetrahedral chains occurs, but the transition from $Ca_2Fe_2O_5$, *Pnma*, to Ca_2FeCoO_5, *Pcmb*, changes the type of chain ordering and therefore yields different space groups and unit cell sizes.[10,11] Also, as described above, the partial substitution of iron by manganese results in a *Pnma* brownmillerite phase for the calcium compound and a disordered $Pm\bar{3}m$ perovskite for the strontium case.

Chromium-substituted phases are also known, but the apparent upper limit for substitution is only 25% of the iron sites in the calcium compound. $Ca_2Fe_{1.5}Cr_{0.5}O_5$ has a brownmillerite structure, *Pnma*,[12,13] and a long-range antiferromagnetic ordering of the G-type with T_c = 455 K. The authors of[12] also identified a phase[14] with composition $Sr_2Fe_{1.5}Cr_{0.5}O_{5.54}$ (y = 0.54 in $Sr_2Fe_{1.5}Cr_{0.5}O_{5+y}$) as a vacancy-disordered cubic phase with a_0 = 3.935 Å, remarkably close to that found here, 3.9449(1) Å. One other single-phase cubic perovskite was also reported as $Sr_2Fe_{1.5}Cr_{0.5}O_{5.11}$ (y = 0.11)[14] with a_0 = 3.917 Å. These results are puzzling because the more oxidized phase, y = 0.54, has a larger cell constant than y = 0.11, an observation in conflict with that expected and normally observed. For example, in the related $Pm\bar{3}m$ defect perovskites, $Sr_2FeMnO_{5.0}$ and $Sr_2FeMnO_{5.5}$, the cell constants are 3.89328(1) and 3.83075(3) Å, respectively.[2] In this case, it was shown that the oxidation pathway is $Mn^{3+} \rightarrow Mn^{4+}$.[2] This expected trend also occurs in the $Sr_2Fe_2O_{5+y}$ series with y = 0.0, 0.50, 0.75, and 1.0, i.e., with an increasing ratio of nominal Fe^{4+}/Fe^{3+}. In these systems, vacancy-ordered structures with large unit cells are found, but they can be compared via the ratio V(cell)/Z, where Z is the number of perovskite formula units in the cell.[8,9,15] The V/Z ratios (Å^3) are 61.10, 57.82, 57.46, and 57.11 for y = 0.0, 0.50, 0.75 and 1.0, respectively. Mössbauer spectra of the reported y = 0.54 and 0.11 phases

dx.doi.org/10.1021/ic202590r | *Inorg. Chem.* 2012, 51, 2638−2644

were interpreted as containing only Fe^{3+}; thus, the oxidation pathway was speculated to be $Cr^{3+} \rightarrow Cr^{4+}$ or Cr^{5+}, not commonly observed oxidation states for chromium in oxides. The Mössbauer data also showed evidence for multiple iron sites, i.e., local atomic ordering and, most remarkably, hyperfine splitting, indicative of long-range or at least short-range magnetic order with possible critical temperatures, T_c, of 463(2) K for $y = 0.11$ and 578 K for $y = 0.54$.[14]

There appear to have been no further studies of these materials. In this article, $Sr_2Fe_{1.5}Cr_{0.5}O_{5+y}$ is synthesized with $y \sim 0$ and the average and local structures are studied. The chromium and iron oxidation states are determined using electron energy-loss spectroscopy (EELS) of the $L_{2,3}$-edges of chromium and iron. Magnetic properties are studied using neutron diffraction to determine the magnetic structure and critical temperature. Comparisons are made with the known $Ca_2Fe_{1.5}Cr_{0.5}O_5$ brownmillerite and other related brownmillerites and oxygen-deficient cubic perovskites.

EXPERIMENTAL SECTION

Synthesis. $Sr_2Fe_{1.5}Cr_{0.5}O_5$ was synthesized using stoichiometric amounts of $SrCO_3$ (99.9% Sigma Aldrich), Fe_2O_3 (99.998% Alfa Aesar), and Cr_2O_3 (99.97% Alfa Aesar). The powders were thoroughly ground, mixed, and pressed into a pellet that was fired at 1280 °C in air, for 36 h followed by quenching in liquid nitrogen, to give a single-phase cubic structure. This follows the procedure used in ref 14 to prepare single-phase cubic $Sr_2Fe_{1.5}Cr_{0.5}O_{5+y}$ phases. A synthesis was also attempted by firing a pellet at 1200 °C in air, followed by slow cooling, which resulted in a poorly crystallized multiphase mixture. If the reaction is performed in an argon atmosphere at 1200 °C, followed by slow cooling, a cubic phase does form but with a smaller unit cell, which is also part of a multiphase mixture. Clearly, this single-phase cubic sample is metastable below 1200 °C.

X-ray and Neutron Diffraction. A PANalytical X'Pert Pro MPD diffractometer with a linear X'Celerator detector was used to collect the X-ray data, with Cu $K\alpha_1$ radiation ($\lambda = 1.54056$ Å) and a 2θ step interval of 0.0084°. Time-of-flight neutron diffraction data at room temperature were obtained on the instrument NPDF at the M. J. Lujan Jr. Center for Neutron Scattering at the Los Alamos Neutron Science Center.[16] Constant-wavelength neutron data were collected on a powder sample in a helium-filled vanadium can at the Canadian Neutron Beam Centre on the C2 diffractometer at 14 different temperatures with a wavelength of 2.3704 Å. Data with $\lambda = 1.32829$ Å were also collected at room temperature and 4 K.

EELS. Samples were deposited from a dispersion of fine powder in ethanol onto a holey carbon grid for investigation.

High-resolution EELS experiments were carried out at the Canadian Centre for Electron Microscopy using a FEI Titan transmission electron microscope, operated at 200 kV. The microscope was operated in diffraction mode with the monochromator excited to provide an energy resolution of 250 meV. Spectra were collected from three different specimens using a GIF Tridiem energy filter, using a convergence angle of ~1 mrad and a collection angle of ~2 mrad. White-line ratio (WLR) measurements were performed using the Pearson method,[17] integrating over 2 eV energy windows for the Fe $L_{2,3}$-edge and 5 eV energy windows for the Cr $L_{2,3}$-edge to allow a direct comparison to values from the literature for both Fe[18] and Cr.[19]

Absolute energy position determination for the Cr and Fe L_3-edges was performed on a JEOL 3000F microscope at the EMAT laboratory operated at 300 kV in diffraction mode. Spectra were collected on a GIF 2000 energy filter using a convergence angle of ~0.9 mrad and an acceptance angle of ~1.2 mrad. To determine the exact edge onset energy, serial low-loss and core-loss spectra were acquired in accordance with the method by Tan et al.[20]

RESULTS AND DISCUSSION

Crystal Structure of $Sr_2Fe_{1.5}Cr_{0.5}O_5$ and the Issue of Oxidation States. A single-phase cubic structure was readily identified from the powder X-ray diffraction data and was refined in a vacancy-disordered $Pm\bar{3}m$ model. The Rietveld refinements were performed by the *GSAS* program suite[21] using the EXPGUI interface.[22] The refinement profiles for the X-ray and neutron diffraction data are shown in Figure 1. Note the presence of magnetic reflections in the neutron data. Considering the large difference between the neutron scattering lengths of iron (9.45 fm) and chromium (3.63 fm), neutron diffraction data were used to determine iron and chromium occupancies. The occupancy of oxygen was also refined using the neutron data. The powder refinement results are shown in Tables 1 and 2.

Table 1. Refinement Results from X-ray (300 K), Time-of-Flight (300 K), and Constant-Wavelength Neutron Diffraction Data (290 K) for $Sr_2Fe_{1.5}Cr_{0.5}O_5$

space group	$Pm\bar{3}m$
lattice parameters	$a = 3.94491(14)$ Å
	$V = 61.392(7)$ Å^3
agreement factors	R_p (X-ray, $\lambda = 1.54056$ Å) = 0.0263
	R_{wp} (X-ray, $\lambda = 1.54056$ Å) = 0.0409
	R_p (neutron, $\lambda = 1.32829$ Å) = 0.0345
	R_{wp} (neutron, $\lambda = 1.32829$ Å) = 0.0450
	R_p (neutron, $\lambda = 2.3704$ Å) = 0.0425
	R_{wp} (neutron, $\lambda = 2.3704$ Å) = 0.0532

Table 2. Atomic Positions, Occupancies, and Thermal Displacement Parameters for $Sr_2Fe_{1.5}Cr_{0.5}O_5$ Obtained from Powder Neutron Diffraction Data, $\lambda = 1.32829$ and 2.3704 Å at 290 K

	x	y	z	occupancy	U_{iso} (Å^2)
Sr	0.5	0.5	0.5	1.0	0.0289(8)
Fe	0	0	0	0.80(1)	0.0229(6)
Cr	0	0	0	0.20(1)	0.0229(6)
O	0.5	0	0	0.842(8)	0.0337(6)
Bond Distance (Å)					
Fe(Cr)−O	1.97245(7)		Sr−Sr	3.94491(14)	
Sr−O	2.78947(7)		Sr−Fe	3.41639(9)	

Refinement of site occupancies show that the compositional formula can be written as $Sr_2Fe_{1.60(3)}Cr_{0.40(3)}O_{5.05(2)}$, where the oxygen content is very close to the ideal value where $y \sim 0.0$, and the Fe/Cr ratio is slightly different but within 3σ of the expected ratio, 1.5/0.5. The refined y value is consistent with trivalent iron and chromium but inconsistent with the value of $y = 0.54$ determined by titration methods for the phase of ref 14 with a very similar cell constant.

Bond valence sum (BVS) calculations[23,24] were performed for $Sr_2Fe_{1.5}Cr_{0.5}O_5$ using normalized parameters, taking into account the contribution of both chromium and iron, proportional to their site occupancies. These calculations result in a valence of 0.551 per Fe(Cr)−O bond, which gives BVS = 2.755, taking an average coordination number of five for the Fe(Cr) site. Note that there is a disorder on the oxygen site. However, even a hypothetical coordination of six will not give a BVS greater than 3.306. These results are consistent with the assumption that the average oxidation state at the Fe(Cr) site is 3+.

dx.doi.org/10.1021/ic202590r | Inorg. Chem. 2012, 51, 2638−2644

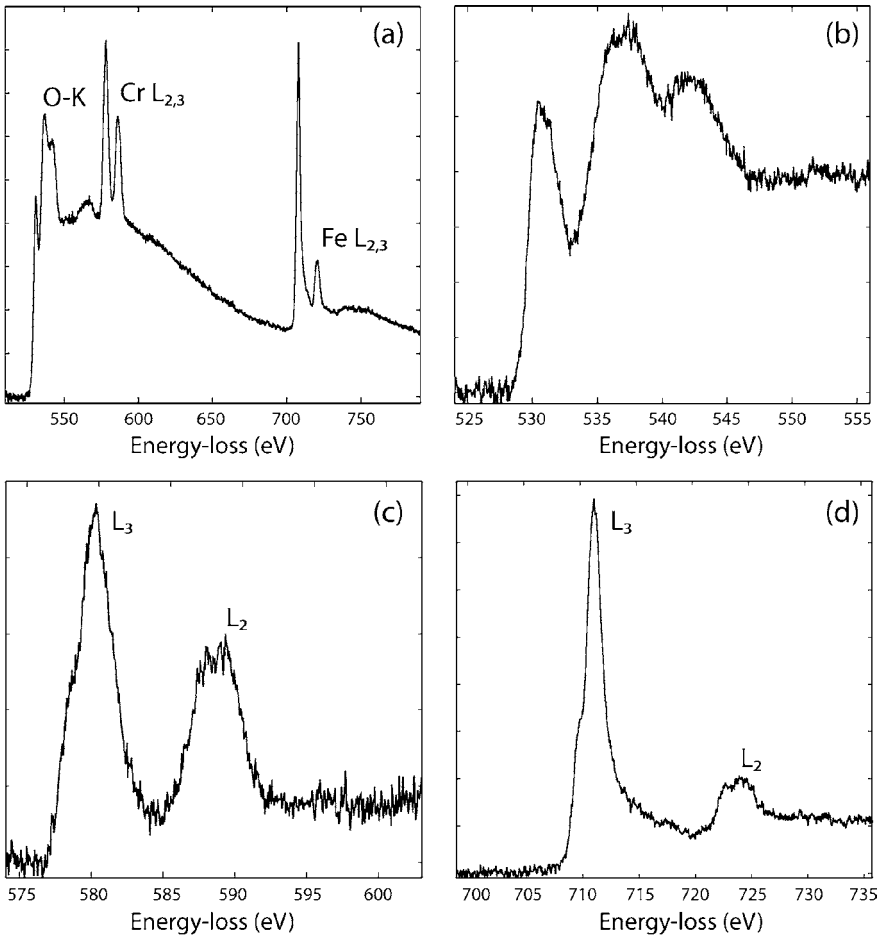

Figure 2. High-resolution EELS spectra for $Sr_2Fe_{1.5}Cr_{0.5}O_5$ showing (a) the O−K, Cr−$L_{2,3}$, and Fe−$L_{2,3}$ edges simultaneously, (b) the O−K edge, (c) the Cr−$L_{2,3}$-edge, and (d) the Fe−$L_{2,3}$-edge.

Further evidence comes from a direct comparison of the unit cell parameters with relevant compounds.[8,9] Consider the unit cell axis of $Sr_2Fe_{1.5}Cr_{0.5}O_5$ reported in this work, a_0 = 3.94491(14) Å, that of $Sr_2FeMnO_{5.0}$, a_0 = 3.89328(1) Å, where the iron and manganese oxidation states are both 3+[2] and that of $Sr_2Fe_2O_6$ ($SrFeO_3$ prepared in high-pressure oxygen), a_0 = 3.851(1) Å.[15] The relevant ionic radii are Cr^{3+} (0.615 Å), $Mn^{3+} \sim Fe^{3+}$ (0.645 Å), Cr^{4+} (0.55 Å), Cr^{5+} (0.49 Å), and Fe^{4+} (0.585 Å).[25] It is difficult to understand the rather large cell constant for the phase prepared here if any combination of Fe^{4+}, Cr^{4+}, or Cr^{5+} exist in large concentrations.

A more definitive measure of the oxidation states can be obtained from spectroscopic methods. As was already mentioned, the Mössbauer data reported in ref 14 for $Sr_2Fe_{1.5}Cr_{0.5}O_{5+y}$ samples with y = 0.11 and 0.54 indicate the presence of Fe^{3+} only. Thus, a determination of the chromium oxidation state is critical along with that for iron in this sample. This was obtained by (1) a comparison of the shape of the acquired Cr and Fe $L_{2,3}$-edge EELS spectra to literature references for the possible oxidation states, (2) a determination of the L_3/L_2 white line ratio (WLR), and (3) an accurate determination of the Cr and Fe L_3-edge onset and peak maximum positions, all parameters that are known to be sensitive to the oxidation state of transition metals.[26] The results are shown in Figure 2. First, an inspection and comparison of the acquired Cr and Fe $L_{2,3}$-edge shapes to the literature[18,27,28] provided an early indication that both species have a valency of 3+. Second, the oxidation states were deduced from the relative L_3/L_2 peak intensities, using a standard Pearson method[17] (see also the Experimental Section). WLR values of 1.62(5) for chromium and 5.7(1) for iron were obtained, which are both in excellent agreement with values for Cr^{3+} and Fe^{3+} in the literature.[19,18] Finally, the edge onset and peak maximum positions for the Cr and Fe L_3-edges were accurately determined. These measurements yielded edge onset and maximum values of 576.9(1) and 580.1(1), respectively, for the Cr L_3-edge and 708.1(1) and 710.8(1), respectively, for the Fe L_3-edge. Again, these values are in excellent agreement with the literature values for Cr^{3+} and Fe^{3+}.[20,27] All three measurements, therefore, identify the oxidation states unambiguously as Cr^{3+} and Fe^{3+}, with the latter in agreement with previous Mössbauer data on a very similar phase.[19,24,29]

Thus, all of the crystallographic and spectroscopic results for the $Sr_2Fe_{1.5}Cr_{0.5}O_{5.05}$ phase prepared in this work are consistent with the coexistence of Fe^{3+} and Cr^{3+} on the perovskite B site and thus $y \sim 0$ in contrast with previous reports.

Before leaving the discussion of the average structure, a comparison between $Sr_2Fe_{1.5}Cr_{0.5}O_5$ and its calcium analogue, brownmillerite *Pnma* $Ca_2Fe_{1.5}Cr_{0.5}O_5$, is also in order.[12,13] Clearly, the substitution of strontium for calcium destroys the brownmillerite ordering. A similar effect was observed for Ca_2FeMnO_5 and Sr_2FeMnO_5.[1,2] However, $Sr_2Fe_{1.5}Cr_{0.5}O_5$

dx.doi.org/10.1021/ic202590r | *Inorg. Chem.* 2012, 51, 2638−2644

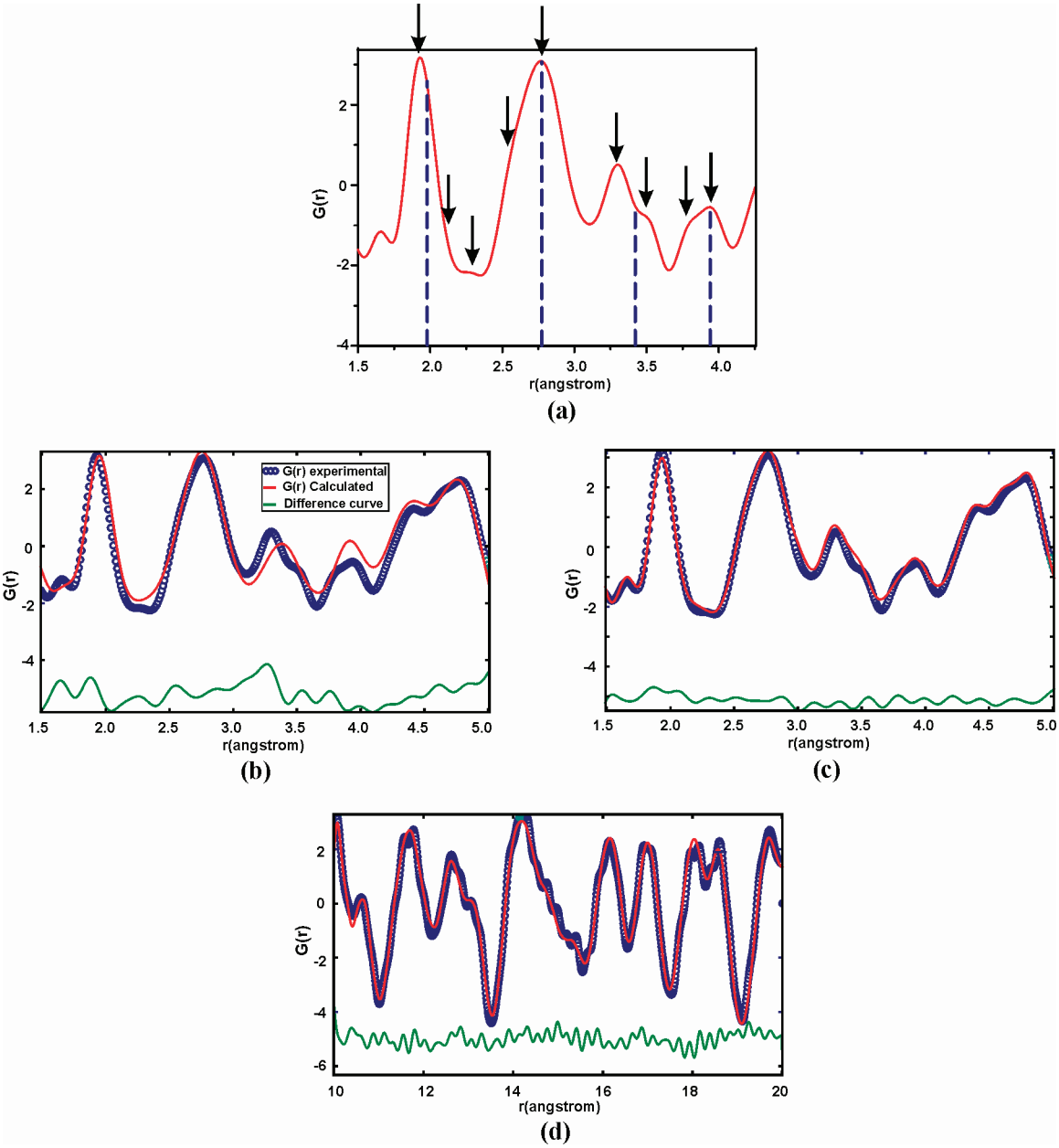

Figure 3. (a) $G(r)$ pattern obtained as described in the text for $Sr_2Fe_{1.5}Cr_{0.5}O_5$ from 1.5 to 4 Å. The purple dashed lines show the expected peak positions for the average structure model, $Pm\bar{3}m$. The arrows show the peaks and shoulders that match a brownmillerite model. (b) $G(r)$ fit using a $Pm\bar{3}m$ model from 1.5 to 5 Å, $R_w = 0.268$. (c) $G(r)$ fit using a brownmillerite *Ibm*2 model from 1.5 to 5 Å, $R_w = 0.127$. (d) $G(r)$ fit using a $Pm\bar{3}m$ model from 10 to 20 Å, $R_w = 0.135$.

appears to be a metastable phase, so comparisons should be made with caution.

Local Structure of $Sr_2Fe_{1.5}Cr_{0.5}O_5$. To explore the local structure of this material, neutron-pair distribution function (NPDF) analysis was performed. This method analyzes the total scattering by taking into account both Bragg peaks and diffuse scattering equally. Powder data are obtained to very large momentum transfer, $Q_{max} = 30$ Å^{-1} in this case, corrected for a number of parameters including the sample can scattering, normalized, and then a sine Fourier transform is carried out to obtain the real-space atomic pair distribution, $G(r)$.[16] The intensity associated with each peak depends on the number of interatomic interactions at a particular distance, r, and the product of the neutron scattering lengths of the atoms involved in that interaction. This can be compared against the interatomic distances expected from the crystal structure obtained from conventional Rietveld refinement, to evaluate the local structure. The $G(r)$ data can also be fitted to particular crystallographic models within a chosen length scale using the *PDFGUI* program.[30]

On the basis of the average structure model, $Pm\bar{3}m$, the interatomic distances (Table 2) that should appear in $G(r)$ up to 4 Å are those shown as dashed lines in Figure 3a. It is clear that this cubic model cannot describe the local structure properly. There are several shoulders and peaks, highlighted by arrows in Figure 3a, that do not match this model. *PDFGUI* refinement from 1.5 to 5 Å with a $Pm\bar{3}m$ model, shown in Figure 3b, results in a poor fit with $R_w = 0.268$.

Careful examination of the $G(r)$ pattern between 1.5 and 5 Å reveals that the features observed in these data match the

dx.doi.org/10.1021/ic202590r | *Inorg. Chem.* 2012, 51, 2638−2644

interatomic interactions expected from a brownmillerite model, with ordering of oxygen vacancies. For example, in the brownmillerite $Sr_2Fe_2O_5$ at 293.15 K[31] several Fe−O interactions occur at distances ranging from 1.820(5) to 2.217(4) Å and Sr−O interactions from 2.473(7) to 2.826(21) Å.

The *PDFGUI* fit with a brownmillerite model (Figure 3c) yields significantly better results with $R_w = 0.127$. Therefore, the local structure is better described by a brownmillerite model, which implies a local ordering of oxygen vacancies as previously suggested by the Mössbauer data.[14] At longer distances, 10−20 Å, the local structure is expected to have more similarities to the average structure, a fact confirmed by the *PDFGUI* refinement (Figure 3d), which shows a reasonable match with the cubic model, $R_w = 0.135$.

Therefore, NPDF results indicate that while the oxygen vacancies are disordered in the long-range sense, there is a short-range brownmillerite-type vacancy ordering in $Sr_2Fe_{1.5}Cr_{0.5}O_5$. A similar result has been observed for Sr_2FeMnO_5.[2] These NPDF results are consistent with the findings of electron diffraction and lattice imaging studies reported for a number of oxygen-deficient cubic or pseudocubic perovskites.[32,33] In these cases, a complex multidomain structure was revealed by electron diffraction/lattice imaging, which involved intergrowths between brownmillerite or partial brownmillerite and perovskite cells. Thus, it is not surprising that a local brownmillerite order would be detected in this material using NPDF methods.

Magnetic Structure of $Sr_2Fe_{1.5}Cr_{0.5}O_5$. As was already mentioned, the neutron diffraction data for $Sr_2Fe_{1.5}Cr_{0.5}O_5$ at 4 and 290 K contain magnetic Bragg peaks, indicating the presence of a long-range magnetic ordering. Seven peaks were detected that could be indexed with propagation vector $\mathbf{k} = (^1/_2, ^1/_2, ^1/_2)$, implying a doubled magnetic cell axis relative to the primitive cubic structural cell. This is consistent with a G-type antiferromagnetic structure, with magnetic moments on each site pointing antiparallel to all nearest neighbors. The two strongest magnetic peaks, indexed as $(^1/_2\ ^1/_2\ ^1/_2)$ and $(^3/_2\ ^1/_2\ ^1/_2)$, are marked by arrows in Figure 1. The magnetic moment per Fe/Cr site obtained from the refinements using *FullProf*[34,35] and *WinPLOTR*[35,36] at 4 K is 3.4(7) μ_B. This value can be compared with a weighted moment of 3.9 μ_B, which is obtained assuming 4.3 μ_B for Fe^{3+} and 2.5 μ_B for Cr^{3+} (values typically found in real oxide materials).

In order to determine T_c, the critical temperature for long-range order, data were taken at several temperatures up to 585 K. From Figure 4, it appears that $T_c \sim 580$ K, roughly consistent with the Mössbauer study,[14] but closer inspection of the data shows that the magnetic reflections begin to broaden significantly above ~560 K, as indicated in the inset. As seen here, the ratio of the full width at half-maximum (fwhm) for $(^1/_2\ ^1/_2\ ^1/_2)/(100)$ more than doubles between 550 and 575 K. Thus, the true T_c is better determined by the sharp increase in the fwhm that occurs between ~565 and 570 K.

Some comments regarding the previous Mössbauer data and the present neutron diffraction study are in order. First, Mössbauer spectroscopy is a local probe, and the observation of hyperfine splitting, while suggestive of long-range magnetic order, is not definitive. For example, in the closely related material $Sr_2FeMnO_{5.0}$, ^{57}Fe hyperfine splitting was observed but neutron diffraction data showed that the magnetic correlations were confined to a domain size of ~50 Å.[2] That the magnetic neutron diffraction peaks are resolution-limited demonstrates the presence of long-range magnetic order in $Sr_2Fe_{1.5}Cr_{0.5}O_{5.05}$ within instrumental resolution.

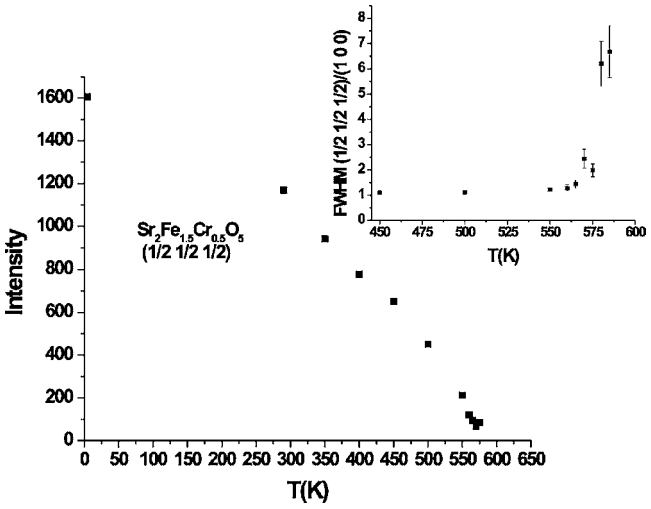

Figure 4. Temperature dependence of the intensity of the $(^1/_2\ ^1/_2\ ^1/_2)$ magnetic reflection. The inset shows the ratio of the fwhm for the $(^1/_2\ ^1/_2\ ^1/_2)/(100)$ reflections.

Finally, recall that the vacancy-ordered calcium analogue, $Ca_2Fe_{1.5}Cr_{0.5}O_5$, is antiferromagnetically ordered with $T_c = 455$ K.[12,13] Therefore, the substitution of strontium for calcium and the consequent destruction of vacancy ordering result in a significant increase in the magnetic transition temperature, although the opposite might be expected because of the high disorder levels present in $Sr_2Fe_{1.5}Cr_{0.5}O_5$. The structural constraints of the calcium analogue that result in large deviations of superexchange pathways from ideal may be, in part, responsible for lowering the T_c for that material. For example, the Fe(Cr)−O−Fe(Cr) angle within the octahedral site plane in $Ca_2Fe_{1.5}Cr_{0.5}O_5$ is 165.4° compared to the corresponding angle for the cubic phase, which is, of course, 180°.

SUMMARY

In summary, the metastable oxygen-deficient perovskite $Sr_2Fe_{1.5}Cr_{0.5}O_5$ was synthesized, and its average structure was found to be a vacancy-disordered $Pm\bar{3}m$ cubic perovskite, while its local structure involves a short-range ordering of oxygen vacancies similar to that of a brownmillerite.

EELS data demonstrate that only trivalent iron and chromium occupy the B-site, which contrasts with a model proposed previously for a material with a very similar unit cell constant.

$Sr_2Fe_{1.5}Cr_{0.5}O_5$ has a long-range antiferromagnetic G-type ordering with $T_N \sim 565$ K, apparent from a sharp increase in the fwhm of the magnetic reflections. This is in reasonable accordance with previously reported Mössbauer data. In cubic oxygen-deficient perovskites, A_2BBO_{6-y}, $y \sim 1$, the combination of vacancy disorder and B-site cation disorder generally destroys long-range magnetic ordering. Therefore, the presence of long-range antiferromagnetism in $Sr_2Fe_{1.5}Cr_{0.5}O_5$ is a remarkable phenomenon.

AUTHOR INFORMATION

Corresponding Author

*E-mail: greedan@mcmaster.ca.

■ ACKNOWLEDGMENTS

J.E.G. acknowledges support of the Natural Sciences and Engineering Research Council (NSERC) of Canada through Discovery Grants. This work has benefited from the use of NPDF at the Lujan Center at Los Alamos Neutron Science Center, funded by DOE Office of Basic Energy Sciences. Los Alamos National Laboratory is operated by Los Alamos National Security LLC under DOE Contract DE-AC52-06NA25396. The upgrade of NPDF has been funded by the NSF through Grant DMR 00-76488. The Canadian Neutron Beam Centre is funded jointly by NSERC and the National Research Council of Canada. The Canadian Centre for Electron Microscopy acknowledges support from the NSERC. S.T. gratefully acknowledges financial support from the Fund for Scientific Research Flanders. H. Tan is gratefully acknowledged for his help with the absolute edge onset energy determination.

■ REFERENCES

(1) Ramezanipour, F.; Cowie, B.; Derakhshan, S.; Greedan, J. E.; Cranswick, L. M. D. *J. Solid State Chem.* **2009**, *182*, 153.
(2) Ramezanipour, F.; Greedan, J. E.; Siewenie, J.; Proffen, Th.; Ryan, D. H.; Grosvenor, A. P.; Donaberger, R. *Inorg. Chem.* **2011**, *50*, 7779.
(3) Rizki, Y.; Bréard, Y.; Le Breton, J.-M.; Folcke, E.; Lechevallier, L.; Kobayashi, W.; Maignan, A. *Solid State Sci.* **2010**, *12*, 1661.
(4) Kashima, N.; Inoue, K.; Wada, T.; Yamaguchi, Y. *Appl. Phys.* **2002**, *A74* (Suppl.), S805.
(5) Cussen, E. J.; Vente, J. F.; Battle, P. D.; Gibb, T. C. *J. Mater. Chem.* **1997**, *7*, 459.
(6) Ricciardo, R. A.; Cuthbert, H. L.; Woodward, P. M.; Zhou, Q.; Kennedy, B. J.; Zhang, Z.; Avdeev, M.; Jang, L.-Y. *Chem. Mater.* **2010**, *22*, 3369.
(7) Berggren, J. *Acta Chem. Scand.* **1971**, *25*, 3616.
(8) D'Hondt, H.; Abakumov, A. M.; Hadermann, J.; Kalyuzhnaya, A. S.; Rozova, M. G.; Antipov, E. V.; Tendeloo, G. V. *Chem. Mater.* **2008**, *20*, 7188.
(9) Greaves, C.; Jacobson, A. J.; Tofield, B. C.; Fender, B. E. F. *Acta Crystallogr.* **1975**, *B31*, 641.
(10) Ramezanipour, F.; Greedan, J. E.; Grosvenor, A. P.; Britten, J. F.; Cranswick, L. M. D.; Garlea, V. O. *Chem. Mater.* **2010**, *22*, 6008.
(11) Battle, P. D.; Gibb, T. C.; Lightfoot, P. *J. Solid State Chem.* **1988**, *76*, 334.
(12) Gibb, T. C.; Matsuo, M. *J. Solid State Chem.* **1990**, *88*, 485.
(13) Battle, P. D.; Bollen, S. K.; Gibb, T. C.; Matsuo, M. *J. Solid State Chem.* **1991**, *90*, 42.
(14) Gibb, T. C.; Matsuo, M. *J. Solid State Chem.* **1990**, *86*, 164.
(15) Hodges, J. P.; Short, S.; Jorgensen, J. D.; Xiong, X.; Dabrowski, B.; Mini, S. M.; Kimball, C. W. *J. Solid State Chem.* **2000**, *151*, 190.
(16) Proffen, T.; Egami, T.; Billinge, S. J. L.; Cheetham, A. K.; Louca, D.; Parise, J. B. *Appl. Phys.* **2002**, *A74*, S163.
(17) Pearson, D. H.; Ahn, C. C.; Fultz, B. *Phys. Rev.* **1993**, *B 47*, 8471.
(18) van Aken, P. A.; Liebscher, B. *Phys. Chem. Miner.* **2002**, *29*, 188.
(19) Arevalo-Lopez, A. M.; Alario-Franco, M. A. *Inorg. Chem.* **2009**, *48*, 11843.
(20) Haiyan, T.; Verbeeck, J.; Abakumov, A.; Van Tendeloo, G. *Oxidation state and chemical shift investigation in transition metal oxides by EELS*; 2011, unpublished work.
(21) Larson A. C.; Von Dreele, R. B. *General Structure Analysis System (GSAS)*; Los Alamos National Laboratory Report LAUR; Los Alamos National Laboratory: Los Alamos, NM, 1994; pp 86−748.
(22) Toby, B. H. *J. Appl. Crystallogr.* **2001**, *34*, 210.
(23) Brown, I. D.; Altermatt, D. *Acta Crystallogr., Sect. B: Struct. Sci.* **1985**, *41*, 244.
(24) *VALENCE* program, /http://www.ccp14.ac.uk/ccp/web-mirrors/i_d_brown/S.
(25) Shannon, R. D. *Acta Crystallogr.* **1976**, *A32*, 751.
(26) Egerton, R. F. *Electron energy-loss spectroscopy in the TEM*; Plenum Press: New York, 1996.
(27) Daulton, T. L.; Little, B. J. *Ultramicroscopy* **2006**, *106*, 561.
(28) Colliex, C.; Manoubi, T.; Ortiz, C. *Phys. Rev.* **1991**, *B 44*, 11402.
(29) Jasinski, J.; Pinkerton, K. E.; Kennedy, I. M.; Leppert, V. *Microsc. Microanal.* **2006**, *12*, 424.
(30) Farrow, C. L.; Juhás, P.; Liu, J. W.; Bryndin, D.; Božin, E. S.; Bloch, J.; Proffen, Th.; Billinge, S. J. L. *J. Phys.: Condens. Matter* **2007**, *19*, 335219.
(31) Schmidt, M.; Campbell, S. J. *J. Solid State Chem.* **2001**, *156*, 292.
(32) Vallet-Regi, M.; Gonzalez-Calbet, J. M.; Verde, J.; Alario-Franco, M. A. *J. Solid State Chem.* **1985**, *57*, 197.
(33) Gonzalez-Calbet, J. M.; Alonso, J.; Vallet-Regi, M. *J. Solid State Chem.* **1987**, *71*, 331.
(34) Rodríguez-Carvajal, J. *Phys. B: Condens. Matter* **1993**, *192*, 55.
(35) Rodriguez-Carvajal, J.; Roisnel, T. *FullProf.98 and WinPLOTR: New Windows 95/NT Applications for Diffraction, Commission for Powder Diffraction*; International Union for Crystallography, Newletter No. 20 (May−August) Summer, 1998.
(36) Roisnel, T.; Rodriguez-Carvajal, J. WinPLOTR: a Windows tool for powder diffraction patterns analysis. In *Proceedings of the Seventh European Powder Diffraction Conference (EPDIC 7), Materials Science Forum*; Delhez, R., Mittenmeijer, E. J., Eds.; 2000; pp. 118−123.